

Essential role of MALAT1 in reducing traumatic brain injury

<https://doi.org/10.4103/1673-5374.332156>

Date of submission: June 13, 2021

Date of decision: September 26, 2021

Date of acceptance: November 4, 2021

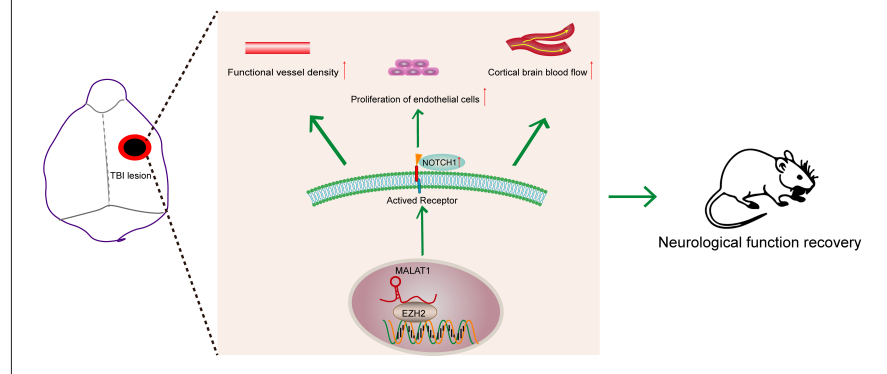
Date of web publication: January 7, 2022

Na Wu^{1, #}, Chong-Jie Cheng^{1, #}, Jian-Jun Zhong¹, Jun-Chi He¹, Zhao-Si Zhang¹, Zhi-Gang Wang¹, Xiao-Chuan Sun¹, Han Liu^{1, 2, *}

From the Contents

Introduction	1776
Materials and Methods	1777
Results	1779
Discussion	1782

Graphical Abstract An experiment demonstrated that MALAT1 could promote angiogenesis following traumatic brain injury via the EZH2-NOTCH1 axis



Abstract

As a highly evolutionary conserved long non-coding RNA, metastasis associated lung adenocarcinoma transcript 1 (MALAT1) was first demonstrated to be related to lung tumor metastasis by promoting angiogenesis. To investigate the role of MALAT1 in traumatic brain injury, we established mouse models of controlled cortical impact and cell models of oxygen-glucose deprivation to mimic traumatic brain injury *in vitro* and *in vivo*. The results revealed that MALAT1 silencing *in vitro* inhibited endothelial cell viability and tube formation but increased migration. In MALAT1-deficient mice, endothelial cell proliferation in the injured cortex, functional vessel density and cerebral blood flow were reduced. Bioinformatic analyses and RNA pull-down assays validated enhancer of zeste homolog 2 (EZH2) as a downstream factor of MALAT1 in endothelial cells. Jagged-1, the Notch homolog 1 (NOTCH1) agonist, reversed the MALAT1 deficiency-mediated impairment of angiogenesis. Taken together, our results suggest that MALAT1 controls the key processes of angiogenesis following traumatic brain injury in an EZH2/NOTCH1-dependent manner.

Key Words: angiogenesis; controlled cortical impact; EZH2; Jagged-1; LncRNA; MALAT1; NOTCH1; oxygen-glucose deprivation; traumatic brain injury; vascular remodeling

Introduction

Traumatic brain injury (TBI) is associated with high morbidity and mortality worldwide. In the past 150 years, the mortality rate of patients with severe TBI has decreased by more than 50% but remains as high as 30% (Stein et al., 2010). Over 30 clinical trials have been carried out, but the outcomes have been unsuccessful. Consequently, effective treatments for TBI remain limited (Diaz-Arrastia et al., 2014; Wright et al., 2014).

Long non-coding RNAs (LncRNAs) are a novel class of RNA with > 200 nucleotides that lack a complete open reading frame. Recently, LncRNAs have been extensively reported to have vital epigenetic regulatory potential (Yao et al., 2019; Di et al., 2021; Liang et al., 2021), but their role in TBI pathology remains unclear. Three independent studies investigated the expression profiles of LncRNA after TBI in the brain tissues of mice, rats and humans (Zhong et al., 2016; Wang et al., 2017; Yang et al., 2019). Several differentially

expressed LncRNAs have been identified to date (Tuchscherer et al., 1992). For example, LncRNA Gm4419 promotes astrocytic apoptosis after TBI by upregulating tumor necrosis factor- α (Yu et al., 2017a). In addition, LncRNA Neat1 inhibits cell apoptosis and inflammation by capturing p53-induced death domain protein 1 following TBI (Zhong et al., 2017). We previously found that metastasis associated lung adenocarcinoma transcript 1 (MALAT1) is one of the most abundant LncRNAs expressed in brain tissue before and after controlled cortical impact (CCI), whereas the functions of other highly expressed LncRNAs were mostly undefined under RNA sequencing (unpublished data). MALAT1, a highly evolutionarily conserved LncRNA with a length of ~8000 nucleotides, was first reported to be related to the metastasis of lung tumors (Ji et al., 2003). MALAT1 overexpression ameliorates brain edema in TBI by inhibiting the nuclear factor kappa-B/interleukin-6 pathway and aquaporin 4 expression (Zhang et al., 2019). Several studies have shown that MALAT1 regulates angiogenesis (Leisegang et al., 2017; Zhang et al., 2018; Wang et al., 2019). Furthermore, MALAT1

¹Department of Neurosurgery, the First Affiliated Hospital of Chongqing Medical University, Chongqing, China; ²Department of Neurosurgery, Qilu Hospital of Shandong University (Qingdao Campus), Qingdao, Shandong Province, China

*Correspondence to: Han Liu, PhD, 1019266517@qq.com.

<https://orcid.org/0000-0001-5726-8751> (Han Liu); <https://orcid.org/0000-0001-8806-2422> (Na Wu)

#Both authors contributed equally to this work.

Funding: The study was supported by the National Natural Science Foundation of China, No. 81571159 (to XCS); the National Natural Science Foundation of China (Youth Program), No. 81601072 (to CJC); and the Natural Science Foundation of Chongqing, China, No. cstc2019jcyj-msxmX0830 (to CJC).

How to cite this article: Wu N, Cheng CJ, Zhong JJ, He JC, Zhang ZS, Wang ZG, Sun XC, Liu H (2022) Essential role of MALAT1 in reducing traumatic brain injury. *Neural Regen Res* 17(8):1776-1784.

modulates endothelial cell function and blood vessel growth (Michalik et al., 2014), but the role of MALAT1 in the cerebral vasculature after TBI requires further clarification.

During the acute phase of TBI, vascular injury disrupts the blood-brain barrier, resulting in hemorrhage and/or edema expansion. The blood-brain barrier is the microenvironment of the central nervous system that allows for proper neuronal function. The properties of the blood-brain barrier are largely attributed to endothelial cells (Daneman and Prat, 2015). Over time, the angiogenic effects promote vascular restoration, including vasculature reconstruction and cerebral blood flow recovery. Therefore, strategies to enhance these effects may provide promising opportunities to improve clinical outcomes for patients with TBI (Salehi et al., 2017). In our study, we aimed to investigate the potential role of MALAT1 in vascular remodeling following TBI and further explore its molecular mechanisms.

Materials and Methods

Animals

Male C57BL/6 mice ($n = 223$, aged 12 weeks, weight 25–30 g) were purchased from the Experimental Animal Center of Chongqing Medical University (Chongqing, China). All mice were housed in cages with food and water available *ad libitum*. All experiments were approved by the Chongqing Medical University Administrative Panel on Laboratory Animal Care on September 25, 2017 (approval No. 2017-147). All experiments were designed and reported in accordance with the Animal Research: Reporting of *In Vivo* Experiments (ARRIVE) guidelines (Percie du Sert et al., 2020). All surgeries were performed under anesthesia, and mice were anesthetized by inhalation with 3% isoflurane (flow rate 3 L/minute, Yuyan Instruments, Shanghai, China) in 67% N₂O/30% O₂ until they did not respond to a tail pinch. Then, 1.5% isoflurane (flow rate 0.5 L/min) was used for anesthesia maintenance.

Experimental design

The experimental process is shown in **Figure 1A**. The grouping of animals was random.

Experiment I

To determine the time course of MALAT1 expression, polymerase chain reaction (PCR) analysis was performed 6 hours and 1, 3, 7, 14, 21 and 28 days after TBI insult ($n = 4$ /time point). To determine MALAT1 localization, fluorescence *in situ* hybridization (FISH) analysis was performed on day 7 following CCI ($n = 4$ /group). For outcome evaluation, mice were divided into sham, sham-siMALAT1, CCI and CCI-siMALAT1 groups ($n = 6$ /group). Neurological severity score (NSS) analyses and wire grip tests were performed *in vivo*. MALAT1 small interfering RNA (siRNA) or negative control siRNA (si-NC) was intracerebroventricularly injected 14 days before TBI modeling.

Experiment II

For angiogenesis evaluation, cell proliferation, tube formation and migration experiments were performed 24 hours after infecting cells with lentivirus siMALAT1 *in vitro*. For the *in vivo* study, mice were divided into sham, sham-siMALAT1, CCI and CCI-siMALAT1 groups ($n = 5$ /group). Immunohistochemical staining of CD31/bromodeoxyuridine (BrdU) and lectin and cerebral blood flow monitoring were performed *in vivo* after the inhibition of MALAT1 with an adeno-associated virus (AAV) on day 7 following CCI.

Experiment III

StarBase software (<https://starbase.sysu.edu.cn/>) was used to predict the interaction probability between MALAT1 and RNA-binding proteins. According to an online RNA-protein interaction prediction database (<http://pridb.gdcb.iastate.edu/RPISeq/>) (Huang et al., 2017), enhancer of zeste homolog 2 (EZH2) exhibited high affinity for MALAT1 (random forest [RF] = 0.95 and support vector machine [SVM] scores = 0.76). First, we found the nucleic acid sequence of EZH2 protein and the nucleotide sequence of MALAT1 through NCBI PubMed. Second, the sequence was entered into StarBase software. The MALAT1-EZH2-NOTCH1 axis was evaluated *in vitro* by western blot 24 hours following oxygen-glucose deprivation (OGD).

Experiment IV

To investigate the mechanism of angiogenesis, cell proliferation, migration and tube formation assays were performed *in vitro* in the presence of Jagged-1 combined with MALAT1 downregulation 24 hours after OGD. Under the same conditions, immunohistochemical

staining of CD31/BrdU and lectin and cerebral blood flow monitoring were performed on day 7 following CCI. The mice were divided into CCI, CCI-siMALAT1 and CCI-siMALAT1 + Jagged-1 groups ($n = 5$ /group).

Experiment V

For outcome evaluation, NSS analyses and wire grip tests were performed *in vivo* in the presence of Jagged-1 combined with MALAT1 downregulation. The mice were divided into CCI, CCI-siMALAT1 and CCI-siMALAT1 + Jagged-1 groups ($n = 6$ /group).

Experiment VI

The effect of MALAT1 on angiogenesis was confirmed by locked nucleic acid (LNA) Gamper (MALAT1 inhibitor) *in vivo* (on day 7 following CCI) and *in vitro* (24 hours following OGD). Mice were divided into CCI and CCI-Gamper groups ($n = 5$ /group).

CCI

According to previous studies (Jiang and Brody, 2012; Zhong et al., 2017; Zhou et al., 2020), CCI was performed to produce a moderately severe contusion in the right sensorimotor cortex and underlying hippocampus, with pronounced behavioral deficits but virtually no mortality. The impact parameters were set as follows: 5.0-m/second velocity, 100-ms dwelling time, 2.0-mm depth and 3.0-mm diameter impactor (Zhong et al., 2017; Zhou et al., 2020). Sham mice underwent craniotomy without CCI. Mice maintained normal body temperature throughout the entire procedure. BrdU (50 mg/kg; MilliporeSigma, Billerica, MA, USA) was first injected intraperitoneally on day 1 post-CCI and then injected daily for 7 consecutive days.

AAV administration

AAV-MALAT1 (GenePharma, Shanghai, China) was used to knock down MALAT1, and AAV-green fluorescent protein (AAV-GFP) was used as a control (Genechem, Shanghai, China). The MALAT1 siRNA sequence was 5'-GCA GTT TAG AAG AGT CTT TAG-3', and the control sequence was 5'-TTC TCC GAA CGT GTC ACG T-3'. Both AAVs were diluted to 1×10^8 transducing units (TU)/mL in enhanced transfection solution (Genechem) before use. The intracerebroventricular injection procedure was performed in accordance with previous studies (Zhu et al., 2005; Zhou et al., 2020). Five microliters of diluted AAV-MALAT1 or AAV-GFP were slowly injected into the lateral ventricle on day 14 before TBI. CCI mice were injected with phosphate buffered saline (PBS).

Cell culture and OGD

Cerebral microvessels were isolated from the brains of male C57BL/6 mice based on a previously reported method (Yin et al., 2006). Cerebral cortices were dissected and homogenized. After centrifugation ($10,000 \times g$ for 5 minutes at 4°C), the precipitates were collected and resuspended in PBS. After the second centrifugation, the precipitates were resuspended in 18% dextroside and centrifuged again ($1500 \times g$ for 20 minutes at 4°C). To avoid contamination from neurons and glial cells in microvascular tissues, the collected precipitates were resuspended in 18% dextroside and centrifuged ($10,000 \times g$ for 1 minute at 4°C). The precipitates were resuspended in PBS and then filtered through a 70- μ m membrane. The filtrate was discarded, and the final vessel pellets were collected and stored at -80°C for biochemical assays. Cells in cerebral microvessels were cultured with Dulbecco's modified Eagle medium (MilliporeSigma) containing 10% fetal bovine serum (Gibco Life Technologies, Grand Island, NY, USA) to confluence. Mouse cerebral vascular endothelial cell cultures were exposed to OGD for various time points (1, 2, 4, 6, 24 and 48 hours) (Yin et al., 2013). The culture medium was replaced with glucose-free Dulbecco's modified Eagle medium (MilliporeSigma), then cells were incubated at 37°C in 5% CO₂. Cells were exposed to OGD for 24 hours.

Lentiviral transfection of endothelial cells

A lentivirus was prepared (GenePharma) to decrease the RNA level of MALAT1. The MALAT1 siRNA sequence was 5'-GGC TAA ACA TCT AGG GTA A-3', and the control sequence was 5'-TTC TCC GAA CGT GTC ACG T-3'. To infect cultured cells with the lentivirus, the virus suspension (100 multiplicity of infection, 0.1 μ L/100 μ L) was added into the culture media based on the most effective titer (siRNA: 5×10^8 TU/mL and control: 1×10^8 TU/mL). The culture medium was replaced with normal medium, and infection continued for 24 hours. Polybrene (Sangon Biotech, Shanghai, China), which enhances infection, was also added into the culture media.

Drugs

Cells were cultured with the EZH2 inhibitor GSK126 (HY-13470, Medchemexpress, New Jersey, USA; 10 μ M, 50 mM in dimethyl sulfoxide). Cells were cultured with the NOTCH1 signaling agonist Jagged-1 (10 μ g/mL; 40A-0157T, Adipogen, San Diego, CA, USA) (Lee et al., 2013). Jagged-1 was injected intraperitoneally at a dose of 400 ng/400 mL *in vivo* (Schmid et al., 2011).

Quantitative RT-PCR (qRT-PCR)

Total RNA from mouse tissue and cultured cells was extracted using Trizol (Invitrogen, Carlsbad, CA, USA) based on the manufacturer's protocol. qRT-PCR was performed using the SYBR Green method. The expression level of mRNA was quantified in duplicate with the Stratagene Mx3005P system (Agilent Technologies, Palo Alto, CA, USA). Each sample was used for the analysis of relative gene expression levels according to the $2^{-\Delta CT}$ formula with $\Delta CT = CT_{\text{target gene}} - CT_{\text{CC1}}$.

RNA-FISH

RNA-FISH was carried out based on the manufacturer's suggestions and a previous study (Wan et al., 2019). Briefly, mice were perfused with 4% formaldehyde in phosphate buffer (pH 7.2). Brains were dissected, post-fixed for 2 hours at 4°C in the same fixative, and then cryoprotected at 4°C in 20% sucrose in phosphate buffer (pH 7.2). Coronal and sagittal sections (10 μ m thick) were made using a cryotome. Fluorescent FISH probe mixes were ordered from commercial sources (RIBOBIO, Guangzhou, China). To achieve a sufficient signal-to-background ratio, multiple probes were targeted along each lncRNA sequence. A set of 15–20 probes covering the entire length of the RNA molecule provided an optimal signal strength, and each probe carried multiple fluorophores. The pooled FISH probes were resuspended to a final concentration of 25 μ M in RNase-free storage buffer and protected from light at –20°C. The endothelium was labeled by von Willebrand factor (1:200, Cat# 27186-1-AP, RRID: AB_2880791, Proteintech, Chicago, IL, USA), and the cell nucleus was labeled by 4,6'-diamidino-2-phenylindole (MilliporeSigma).

NSS and wire grip test

NSS analyses and wire grip tests were performed in accordance with previous research (Flierl et al., 2009; Wang et al., 2013; Zhong et al., 2017; Zhou et al., 2020). Briefly, the NSS measured general behavior, alertness, balance and motor ability, including ten different tasks. One point was obtained for each failed task. Zero points represented the minimum deficit, and ten points represented the maximum deficit. Wire grip tests were used to evaluate vestibular motor function. The apparatus consisted of a stainless-steel bar (50-cm length; 2-mm diameter) mounted on two vertical supports and elevated 37 cm above a flat surface. Mice were placed on the bar midway between the supports and were observed for 60 seconds. A five-point scale was used. Zero points represented the maximum deficit, and five points represented the minimum deficit. Mice were evaluated on the pre-injury day and days 1, 3, 7, 14, 21 and 28 after CCI.

Construction of pcEZH2 overexpression plasmid

To verify the downstream effect of EZH2, the recombinant plasmid pcDNA3.1(+)-EZH2 overexpressing EZH2 was constructed (termed pcEZH2). The DNA MiniPrep or MidiPrep Kit (QIAGEN, Dusseldorf, Germany) was used to prepare plasmid vectors (pcDNA3.1(+)-EZH2 and empty vector pcDNA3.1-GFP) for cell transfection (endothelial cells cultured in a six-well plate) via Lipofectamine 2000 (Invitrogen) in accordance with the manufacturer's instructions. The overexpression efficiency was detected by western blot analysis or real-time qRT-PCR 48 hours after transfection.

LNA GapmeR transfection *in vitro* and *in vivo*

Endothelial cells were transfected at 60–75% confluence with 100 nM synthesized siRNAs (MilliporeSigma) or 1–100-nM LNA GapmeR (Exiqon, Vedbaek, Denmark) targeting MALAT1 using Lipofectamine RNAiMax (Life Technologies, Carlsbad, CA, USA) in accordance with the manufacturer's protocol. As controls, scrambled LNA GapmeR or siFirefly luciferase was transfected. Four hours after transfection, the medium was replaced by EBM (Lonza, Basel, Switzerland) supplemented with EGM-SingleQuots (Lonza) and 10% fetal calf serum (Invitrogen).

LNA GapmeR was dissolved and diluted in nuclease-free, sterile water in accordance with the manufacturer's protocol. LNA GapmeR MALAT1 (20 mg/kg; Exiqon) or LNA GapmeR Ctrl (20 mg/kg; Exiqon)

was injected intravenously pre- and post-surgery as described (Michalik et al., 2014).

Cell viability assay

Endothelial cells (1×10^4 cells/well) were seeded in a 96-well plate, and the number of viable cells was detected using Cell Counting Kit-8 (Dojindo Molecular Technologies, Gaithersburg, MD, USA) following the manufacturer's suggestions. Each well received 10 μ L Cell Counting Kit-8. The number of living cells was assessed by measuring the absorbance at 450 nm at 24 hours. Cell viability (%) was calculated as follows: experimental group absorbance value/control group absorbance value \times 100. The sham group is the control group in our experiments.

Scratch wound assay

Endothelial cells (1×10^5 cells/well) were seeded in a six-well plate. The plates were coated with human fibronectin (1 μ g/mL, MilliporeSigma) overnight at room temperature. Then, cells were detached with trypsin after 24 hours and incubated overnight in 5% CO₂ at 37°C. The next day, the cell monolayer was rinsed once with PBS. Micrographs of wounds were obtained at 0 and 24 hours using a Zeiss Observer Z1 microscope (Leica, Wetzlar, Germany). ImageJ V1.8.0 software (National Institutes of Health, Bethesda, MD, USA) was used to assess the mean migration distance.

Tube formation assay

The tube formation of endothelial cells was assessed using an *in vitro* Angiogenesis Assay Kit (Chemicon, Temecula, CA, USA). Endothelial cells were seeded at 5×10^5 cells/10-cm plate. After 24 hours, the conditioned medium was harvested and filtered via a 0.2- μ m filter (Sartorius Stedim Biotech, Göttingen, Germany). Endothelial cells were cultured in a CO₂ incubator for 24 hours at 37°C. Cultures were photographed (40 \times magnification), and the number of tubes was calculated.

Endothelial cell proliferation *in vivo*

Brain sections (10 μ m) were fixed in 4% paraformaldehyde, then blocked with 5% fetal bovine serum for 80 minutes. The slices were incubated overnight at 4°C with mouse monoclonal anti-CD31 (1:100, Cat# ab24590, RRID:AB_448167, Abcam, Cambridge, UK) and rabbit polyclonal anti-BrdU (1:200, Cat# ab152095, RRID: AB_2813902, Abcam). Slides were washed and incubated at room temperature for 2 hours with the appropriate secondary antibodies, including DyLight 594 goat anti-mouse IgG (1:200, Cat# ab96881, RRID: AB_10680252, Abcam) and DyLight 488 goat anti-rabbit IgG (1:200; Cat# ab96899, RRID: AB_10679361, Abcam). Slices were analyzed using a fluorescence microscope (Leica). Angiogenesis was evaluated by calculating the number of CD31/BrdU double-positive cells in perilesion areas of ipsilateral hemispheres (cortex and subcortex).

Quantification of blood vessel density

Briefly, lectin dye (0.2 mg/mL, Vector Laboratories, Burlingame, CA, USA) in a volume of 300 μ L was given via tail vein injection and allowed to circulate for 10 minutes before sacrifice. Brain sections were examined under a fluorescence microscope. Functional vessel density was evaluated by the area ratio of lectin-positive blood vessels in the cortex and subcortex surrounding the injury site.

Two-dimensional laser speckle imaging techniques

Cerebral blood flow is defined as the amount of arterial blood per unit mass delivered to brain tissue per unit time and is a sensitive physiological index reflecting cerebrovascular function (Joris et al., 2018). Cerebral blood flow was monitored using laser speckle techniques (PeriCam PSI System; Perimed, Stockholm, Sweden) following previous reports (Li et al., 2013; Mao et al., 2017; Liu et al., 2018). Briefly, the camera head was adjusted to ensure that the red cross-point of the indicator laser (660 nm) was located at the center of the brain, and the measurement distance was set at 10 cm. The size of the test area was adjusted with PIM Software version 1.5 (PeriCam PSI System). Cerebral blood flow signals were collected at 785 nm and transferred into blood perfusion images using PIM Software. Perfusion images were acquired using a PeriCam high resolution LSCI system (PeriCam PSI System) with a 70-mW built-in laser diode for illumination and a CCD camera (PeriCam PSI System) on days 1, 3, 7, 10, 14, 21 and 28 post-TBI. The scanner was positioned to scan a 1.5-cm \times 1.5-cm area (1600 detection points), covering the cross-point of the coronal and sagittal sutures. A built-in photo detector equipped with LDPI Win software (PeriCam PSI System) was used to detect the reflected light from moving blood

cells within a depth of 0.5 cm from the cortical surface. Color-coded images were acquired three times continuously, and the average cerebral blood flow was calculated based on the concentration and mean velocity of the blood cells using LDPI Win software. The cerebral blood flow for the ipsilateral side was calculated as a percent of the corresponding contralateral side.

Western blot analysis

Western blot analysis was performed as previously described (Huang et al., 2016; Zhou et al., 2020). Briefly, endothelial cells were collected for total protein extraction. The sample proteins (20 µg/lane) were separated in 10% sodium dodecyl sulfate-polyacrylamide gels (Invitrogen) and transferred onto polyvinylidene fluoride membranes (Millipore, Boston, MA, USA). Membranes were blocked with 5% non-fat milk for 1 hour at room temperature, then incubated overnight at 4°C with primary antibodies, including rabbit monoclonal anti-β-actin (1:5000, Cat# ab213262, Abcam), rabbit polyclonal anti-β-actin (1:5000, Cat# 20536-1-AP, RRID:AB_10700003, Proteintech), rabbit polyclonal anti-EZH2 (1:1000, Cat# 5246, RRID:AB_10694683, Cell Signaling Technology, Danvers, MA, USA), rabbit monoclonal anti-hairy and enhancer of split 1 (HES1; 1:1000, Cat# ab108937, RRID:AB_10862625, Abcam) and rabbit monoclonal anti-NOTCH1 (1:1000, Cat# ab52627, RRID:AB_881725, Abcam). After being washed with Tris-buffered saline/Tween-20, membranes were incubated for 1 hour at room temperature with horseradish peroxidase-conjugated AffiniPure goat anti-rabbit IgG (1:5000; Cat# SA0001-2, RRID:AB_2722564, Proteintech). Enhanced chemiluminescence was used to detect proteins in the membranes (ECL Plus, Millipore), and proteins were quantified using the Fusion system (Fusion fx 7 Spectra, Vilber, France).

RNA pull-down

RNA pull-down was performed as previously described (Huang et al., 2017). Briefly, MALAT1 transcripts were transcribed using T7 RNA polymerase (Ambion Life) *in vitro*. RNA was purified with the RNeasy Plus Mini Kit (QIAGEN), then treated with DNase I (QIAGEN). Purified RNAs were biotin-labeled using Biotin RNA Labeling Mix (Roche Diagnostics, Indianapolis, IN, USA). The biotinylated RNAs were mixed and incubated with endothelial cell lysates. Then, magnetic beads were added to each binding reaction, and the mixtures were incubated at room temperature. Finally, the eluted proteins were identified through western blot analysis.

Statistical analysis

No statistical methods were used to predetermine sample sizes; however, our sample sizes are similar to those reported in previous publications (Ji et al., 2003; Jaé and Dimmeler, 2015). No animals or data points were excluded from the analysis. All quantitative data are shown as the mean ± standard error of the mean (SEM). The neurological behavioral data were analyzed using two-way repeated-measures analysis of variance (Delbary-Gossart et al., 2016), followed by Tukey's *post hoc* test across groups. The qRT-PCR data of MALAT1 and EZH2 *in vivo* were analyzed by one-way analysis of variance, followed by Dunnett's *post hoc* test. Other data tested in three or four experimental groups were analyzed by one-way analysis of variance, followed by Tukey's *post hoc* test. Data tested in only two groups were analyzed by Student's *t*-test. All data were analyzed with Graphpad Prism7.0 software (GraphPad Software, San Diego, CA, USA). The level of statistical significance was set at $P < 0.05$.

Results

MALAT1 expression profile following TBI

In our previous study (Zhong et al., 2016), global lncRNA expression was evaluated before and after CCI, and MALAT1 was one of the highly expressed lncRNAs. Here, we found that the MALAT1 level in the injured cortex rapidly increased as early as 6 hours after CCI ($P < 0.001$), then gradually decreased to the lowest level at 7 days after CCI ($P < 0.001$; **Figure 1B**). The MALAT1 level was increased in cultured endothelial cells at 24 hours after OGD ($P < 0.05$; **Figure 1C**). RNA-FISH analysis showed that MALAT1 immunoreactive cells were located in the cortical endothelium in model mice (**Figure 1D**).

MALAT1 deficiency aggravates neurobehavioral deficits after CCI

To determine the effects of MALAT1 on functional outcomes after CCI, we compared the NSS and wire grip test results (**Figure 1E** and **F**). After CCI, significant neurological impairments were observed in the CCI group compared with the sham group ($P < 0.05$; **Figure 1E** and **F**). Based on the NSS, CCI-siMALAT1 animals developed more severe sensorimotor deficits compared with the CCI group ($P < 0.05$;

Figure 1E). In the wire grip test, the CCI-siMALAT1 group exhibited deteriorated motor performance compared with the CCI group ($P < 0.05$, **Figure 1F**).

MALAT1 downregulation disrupts angiogenesis following TBI

Here, we explored the potential effects of MALAT1 on cerebral angiogenesis. We found that endothelial proliferation and migration were affected after OGD and CCI ($P < 0.05$; **Figure 2A–F**). Endothelial cell viability ($P < 0.05$; **Figure 2A**) and tube formation ($P < 0.05$; **Figure 2B**) were decreased in the sham-siMALAT1 group compared with the sham group. MALAT1 inhibition suppressed endothelial proliferation and tube formation but promoted endothelial migration ($P < 0.05$; OGD-siM group vs. OGD group; **Figure 2A–C**). More importantly, we found that MALAT1 enhanced endothelial proliferation (day 7), functional vessel density (day 21) and cerebral perfusion (day 7) in the lesion areas following CCI ($P < 0.05$, CCI-siMALAT1 group vs. CCI group; **Figure 2D–F**).

EZH2 and NOTCH1 act downstream of MALAT1 in TBI neuropathologies

EZH2 exhibited a high affinity for MALAT1 (RF = 0.95 and SVM = 0.76). This binding probability was further supported by StarBase (**Figure 3A**). As a key regulator of tumor angiogenesis, EZH2 is predominantly upregulated in cancer-derived endothelium, promoting endothelial tube formation (Crea et al., 2012). To investigate the potential interaction between MALAT1 and EZH2, an RNA pull-down assay was performed to evaluate their binding in endothelial cells. The results confirmed the association between EZH2 and MALAT1 ($P < 0.05$; RNA-S vs. RNA-AS; **Figure 3B**). EZH2 expression was markedly suppressed by siMALAT1, indicating the presence of crosstalk between EZH2 and MALAT1. Following CCI, the transcriptional level of EZH2 increased as early as 6 hours and then gradually decreased to low levels at 7 days compared with the sham group. The decreased levels were maintained in the late phase ($P < 0.05$; **Figure 3C**).

Previous studies reported the involvement of NOTCH1 in vascular events. For instance, the miR-32-5p/NOTCH1 axis was found to promote angiogenesis in chronic compressive spinal cord injury (Cheng et al., 2020). Following cerebral ischemia, upregulated NOTCH1 signaling was observed, and NOTCH1 deficiency inhibited local angiogenic activity (Ren et al., 2018). Recently, EZH2 was reported to directly bind to the NOTCH1 promoter and induce its transcription (Gonzalez et al., 2014). Thus, we proposed a hypothesis that the NOTCH1 pathway is involved in MALAT1-EZH2 regulation. EZH2, NOTCH1 and HES1 expression levels were detected by western blot after MALAT1 downregulation in cultured endothelial cells. Our results showed that NOTCH1/HES1 and EZH2 expression were suppressed in the OGD-siM group compared with the OGD group ($P < 0.05$; **Figure 3D**). The NOTCH1 pathway was suppressed by the EZH2 inhibitor ($P < 0.05$; OGD-GSK126 group vs. OGD group; **Figure 3E**), but these effects were reversed by pcEZH2 ($P < 0.05$, OGD-siM group vs. OGD-siM + pcEZH2 group; **Figure 3F**).

NOTCH1 is required in MALAT1-mediated angiogenesis and functional recovery

To investigate the role of the NOTCH1 pathway in vascular regulation, we tested the angiogenic events following TBI based on previously reported methods (Williams et al., 2006; Brüttsch et al., 2010). As shown in **Figure 4**, the effects of MALAT1 on endothelial proliferation, migration and tube formation after OGD were reversed by activation of the NOTCH1 signaling pathway (Jagged-1) ($P < 0.05$; OGD-siM + Jagged-1 group vs. OGD-siM group; **Figure 4A–C**). Endothelial proliferation (day 7), functional vessel density (day 21) and cortical perfusion (day 7) surrounding lesion areas following CCI were enhanced by Jagged-1 even in the absence of MALAT1 ($P < 0.05$; CCI-siM + Jagged-1 group vs. CCI-siM group; **Figure 4D–F**). Furthermore, Jagged-1 rescued the effects of MALAT1 on sensorimotor performances (NSS and wire grip test) ($P < 0.05$; CCI-siM + Jagged-1 group vs. CCI-siM group; **Figure 5A** and **B**).

To validate our results, we performed the above experiments in the presence of the MALAT1 inhibitor LNA GapmeR (Michalik et al., 2014). Consistent with our preliminary findings, GapmeR suppressed angiogenic tube formation and endothelial proliferation and promoted endothelial migration *in vitro* ($P < 0.05$; OGD-GapmeR group vs. OGD group; **Figure 6A–C**). Similarly, GapmeR inhibited endothelial proliferation (d7) and functional vessel density (d21) following CCI ($P < 0.05$; CCI-GapmeR group vs. CCI group; **Figure 6D** and **E**).

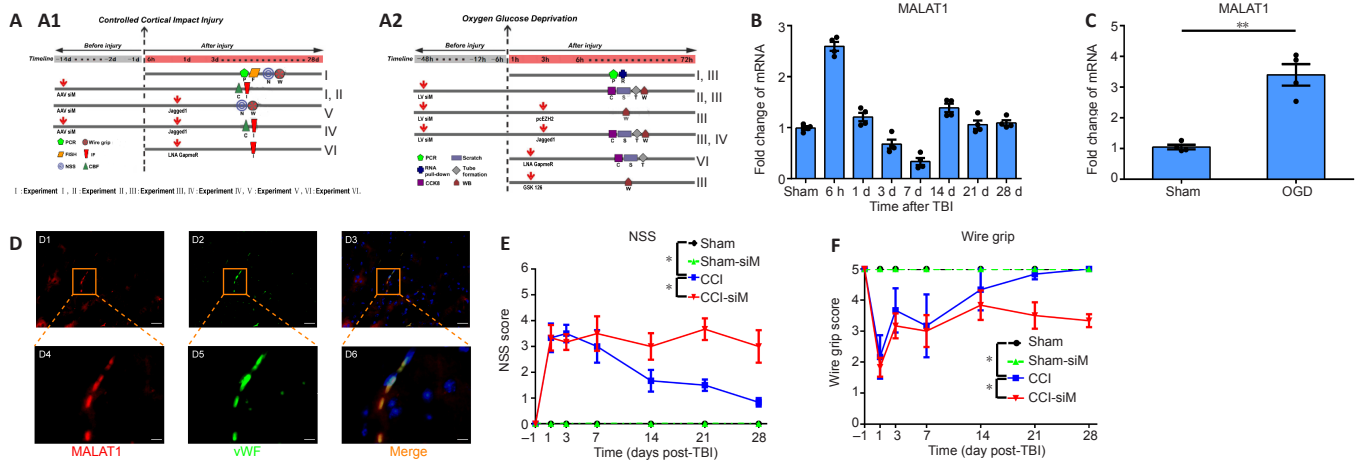


Figure 1 | MALAT1 expression profile and the effects of MALAT1 on neurological function.

(A) Experimental design *in vivo* (A1) and *in vitro* (A2). (B) MALAT1 mRNA expression in brain tissue was detected by qRT-PCR at 6 hours and 1, 3, 7, 14, 21 and 28 days after CCI. The MALAT1 mRNA level rapidly increased as early as 6 hours after CCI, then gradually decreased to the lowest level at 7 days after CCI. (C) MALAT1 mRNA expression was detected at 24 hours after OGD by qRT-PCR. The MALAT1 level was increased in the OGD group compared with the sham group. (D) *In situ* hybridization detection of MALAT1 *in vivo*. MALAT1 (red, DyLight 594) co-localized with vWF (green, DyLight 488). Scale bars: 25 μ m in D1–3, and 10 μ m in D4–6. (E) The NSS. Zero points represented the minimum deficit, and ten points represented the maximum deficit. (F) The wire grip tests. Zero points represented the maximum deficit, and five points represented the minimum deficit. Data are shown as the mean \pm SEM ($n = 4$ /group in B–D, $n = 6$ /group in E–F). * $P < 0.05$, ** $P < 0.01$, *** $P < 0.001$ (one-way analysis of variance followed by Dunnett's *post hoc* test in B, Student's *t*-test in C or two-way repeated-measures analysis of variance followed by Tukey's *post hoc* test in E–F). AAV: Adeno-associated virus; CBF: cerebral blood flow; CCI: controlled cortical impact; CCK8: Cell Counting Kit-8; EZH2: enhancer of zeste homolog 2; FISH: fluorescence in situ hybridization; GSK126: MALAT1 inhibitor; IF: immunofluorescence; Jagged-1: NOTCH1 signaling agonist; LNA: locked nucleic acid; LV: lentivirus; MALAT1: metastasis associated lung adenocarcinoma transcript 1; NSS: neurological severity score; OGD: oxygen-glucose deprivation; pcEZH2: recombinant plasmid pcDNA3.1(+)-EZH2 of overexpressing EZH2; PCR: polymerase chain reaction; qRT-PCR: quantitative reverse transcription polymerase chain reaction; siM: small interfering RNA-metastasis associated lung adenocarcinoma transcript 1; TBI: traumatic brain injury; vWF: von willebrand factor; WB: western blot.

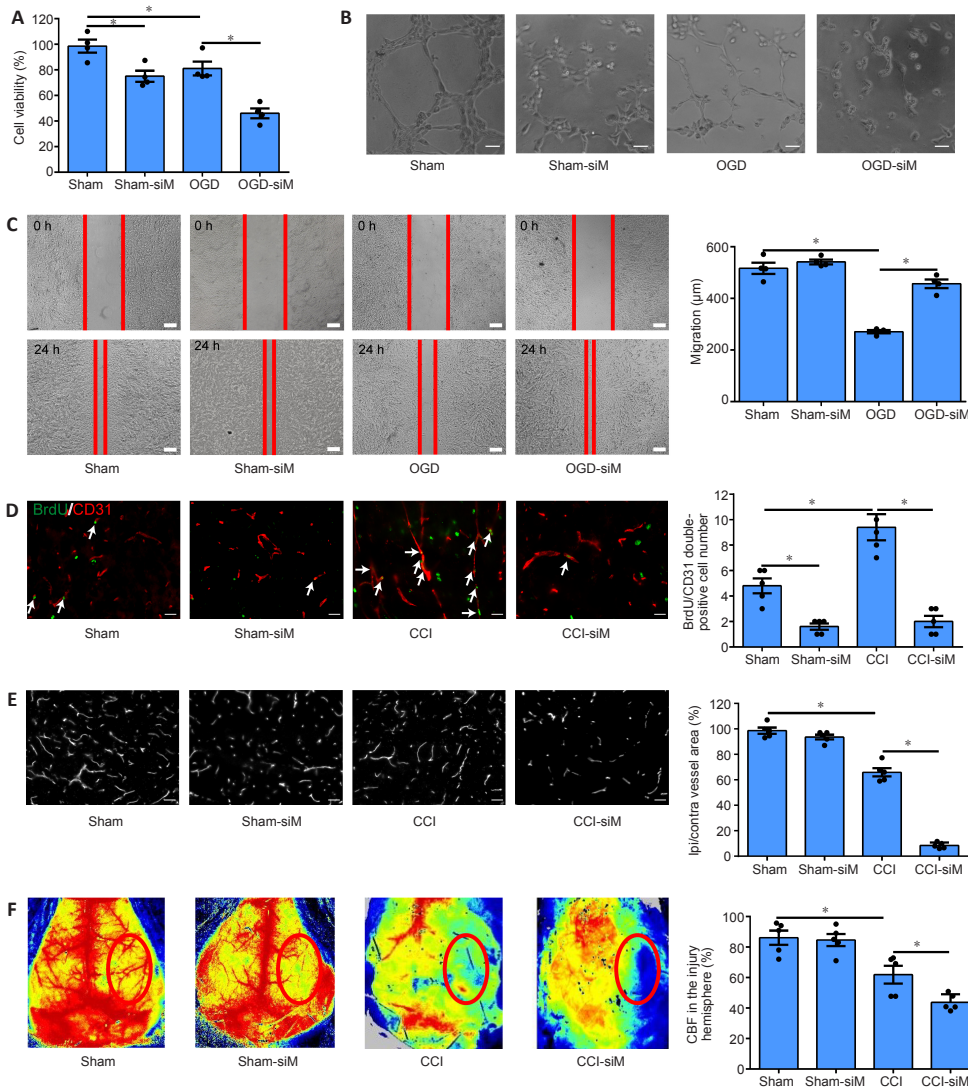
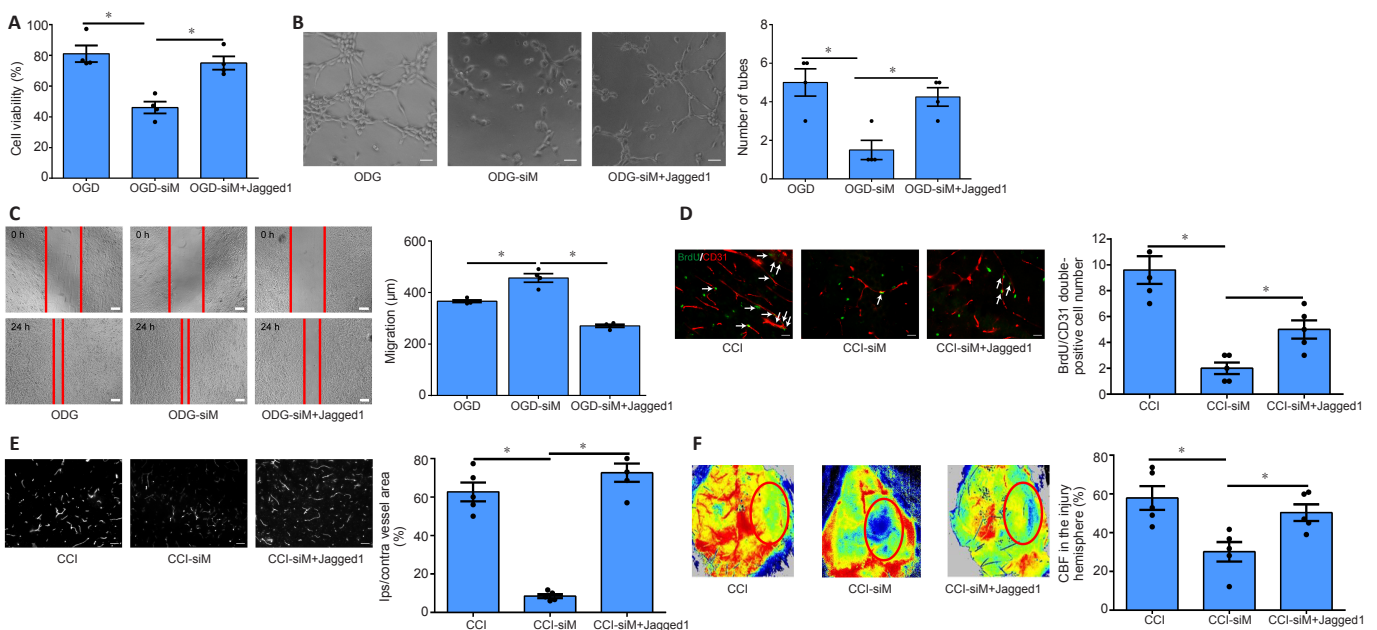
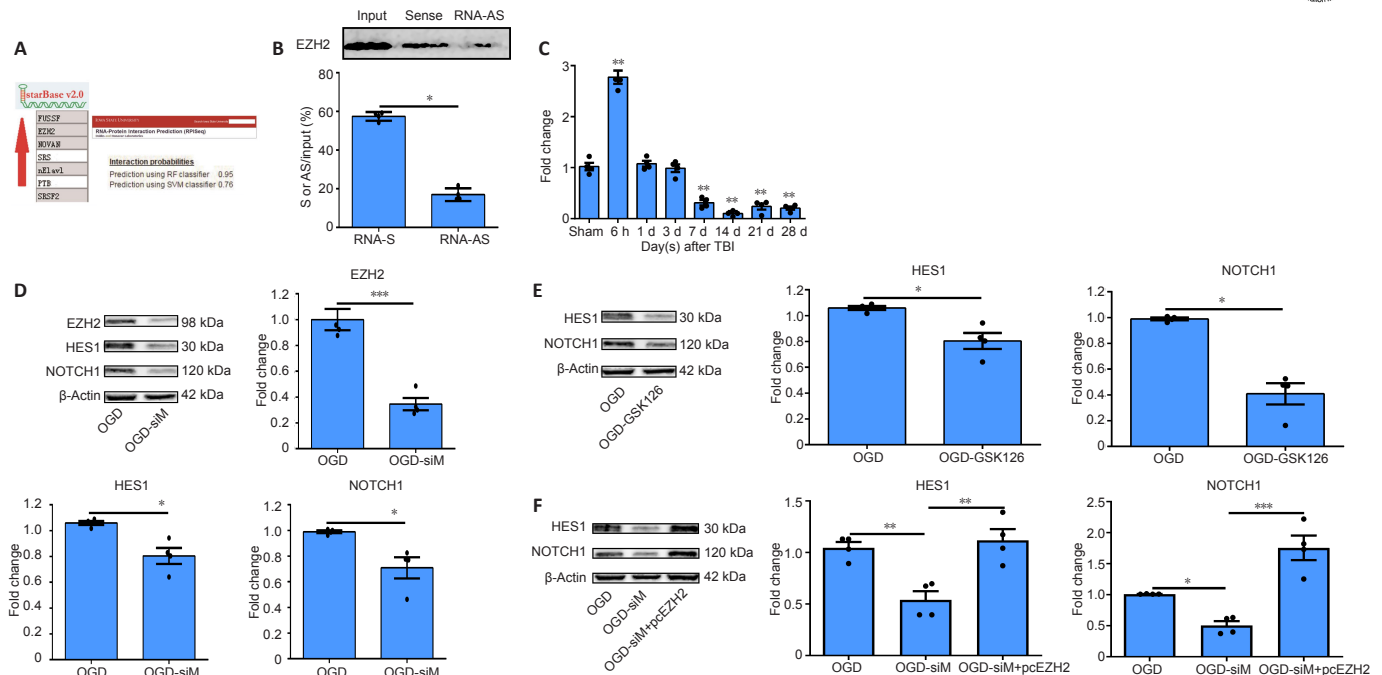


Figure 2 | Effects of siRNA-mediated MALAT1 silencing on angiogenesis *in vitro* and *in vivo*.

Cell viability (by Cell Counting Kit-8) (A), tube formation assay (B) and scratch wound assay (C) after OGD. (D–F) Effects of siMALAT1 on angiogenesis following CCI. The inhibition of MALAT1 suppressed endothelial proliferation and tube formation but promoted endothelial migration. (D) Double immunohistochemical staining of BrdU (green, DyLight 488, a marker of cell proliferation)/CD31 (red, DyLight 594, localized to positive endothelial cells) at 7 days following CCI. The number of BrdU/CD31 double-positive cells was significantly lower in the CCI-siM group compared with the CCI group. Arrows indicate the BrdU/CD31 double-positive cells. (E) Functional vessel density was identified by the staining of perfused lectin at 21 days following CCI. Functional vessel density was significantly lower in the CCI-siM group compared with the CCI group. Scale bars: 50 μ m in B, 200 μ m in C, 25 μ m in D and 12.5 μ m in E. (F) Effect of siMALAT1 on perfusion efficiency at the injury site 7 days following CCI, which was represented by two-dimensional laser speckle images of CBF changes (% CBF relative to contralateral hemisphere). CBF was significantly lower in the CCI-siM group compared with the CCI group. Circles indicate the CBF in lesion areas. Data are expressed as the mean \pm SEM ($n = 4$ /group in A–C, $n = 5$ /group in D–F). * $P < 0.05$ (one-way analysis of variance followed by Tukey's *post hoc* test). BrdU: Bromodeoxyuridine; CBF: cerebral blood flow; CCI: controlled cortical impact; MALAT1: metastasis associated lung adenocarcinoma transcript 1; OGD: oxygen-glucose deprivation; siM/siMALAT1: small interfering RNA-metastasis associated lung adenocarcinoma transcript 1.



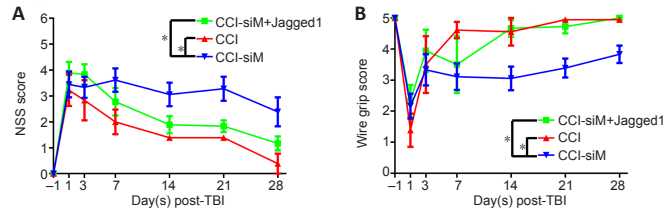


Figure 5 | MALAT1 promotes neurological function through the NOTCH1 signaling pathway *in vivo*.

(A) NSS: Higher points represent more serious deficits. (B) Wire grip tests: Higher points represent less serious deficits. Data are expressed as the mean \pm SEM ($n = 6$ /group). * $P < 0.05$ (two-way repeated-measures analysis of variance followed by Tukey's *post hoc* test). CCI: Controlled cortical impact; NSS: neurological severity score; siM: small interfering RNA-metastasis associated lung adenocarcinoma transcript 1; TBI: traumatic brain injury.

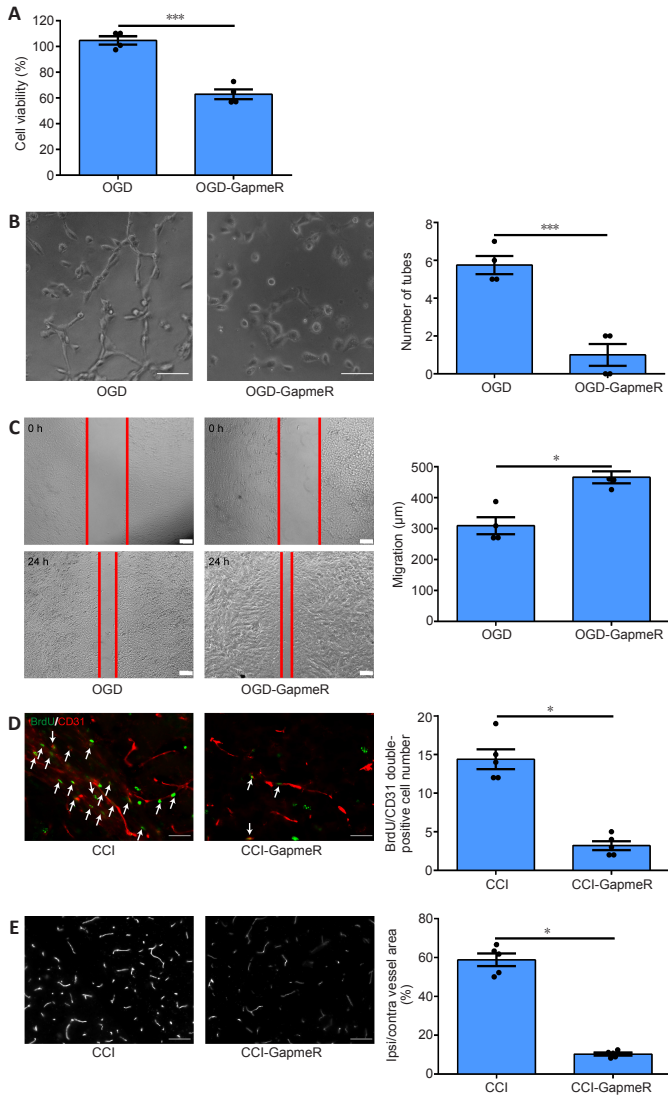


Figure 6 | Effects of LNA GapmeR-mediated inhibition of MALAT1 on angiogenesis *in vitro* and *in vivo*.

Cell viability (by Cell Counting Kit-8) (A), tube formation assay (B) and scratch wound assay (C) after OGD. GapmeR suppressed angiogenic tube formation and endothelial proliferation and promoted endothelial migration. (D, E) Effects of GapmeR on angiogenesis following CCI. (D) Double immunohistochemical staining of BrdU (green, DyLight 488, a marker of cell proliferation)/CD31 (red, DyLight 594, localized to positive endothelial cells) at 7 days following CCI. The number of BrdU/CD31 double-positive cells was significantly lower in the CCI-GapmeR group compared with the CCI group. Arrows indicate the BrdU/CD31 double-positive cells. (E) Functional vessel density was identified by the staining of perfused lectin in different groups at 21 days following CCI. Functional vessel density was significantly lower in the CCI-GapmeR group compared with the CCI group. Scale bars: 50 μ m in B, 200 μ m in C, 25 μ m in D and 12.5 μ m in E. Data are shown as the mean \pm SEM ($n = 4$ /group in A–C, $n = 5$ /group in D and E). * $P < 0.05$, *** $P < 0.001$ (Student's *t*-test). BrdU: Bromodeoxyuridine; CCI: controlled cortical impact; LNA: locked nucleic acid; OGD: oxygen-glucose deprivation.

Discussion

Here, we established a TBI model in experimental mice and cultured cells and performed serial experiments to explore the role of MALAT1 in TBI pathologies. Our data showed that MALAT1 expression was altered in the injured brain hemisphere following CCI and cultured endothelial cells following OGD. MALAT1 downregulation using siRNA and a MALAT1 inhibitor (LNA GapmeR) was associated with decreased angiogenic activities, vasculature growth and cerebrovascular perfusion. Mechanistically, we found that MALAT1 promotes angiogenesis by regulating NOTCH1 after binding to EZH2. For technical reasons, a MALAT1 overexpression AAV could not be constructed. Therefore, this study only verified the hypothesis by inhibiting MALAT1. The effect of MALAT1 on other differentiation pathways of neural stem cells was not discussed.

Several studies have demonstrated that enhanced angiogenesis plays a crucial role in secondary brain injury after TBI (Sköld et al., 2005, 2006; Mueller et al., 2007; Chen et al., 2013). As reported in the literature (Ren et al., 2019; Akil et al., 2021), functional angiogenesis, pathological angiogenesis, and de novo arteriogenesis refer to the growth of new capillaries. Arteriolar blood vessels in the brain might be critical for repairing brain injury after TBI. Therefore, strategies based on enhancing angiogenesis might provide therapeutic potential for TBI. lncRNAs have emerged as key regulators of diverse cellular processes (Sun and Kraus, 2015), including some closely associated with angiogenesis (Thum and Fiedler, 2014; Fiedler et al., 2015; Jaé and Dimmeler, 2015; Beermann et al., 2016; van Kruijsdijk et al., 2016). Recent evidence indicated that lncRNA MALAT1 played an important role in regulating angiogenesis in tumors (Tee et al., 2016) and peripheral vessels (Michalik et al., 2014). MALAT1 was also reported to increase resistance to apoptosis and inflammation induced by experimental ischemic stroke (Zhang et al., 2017). Similarly, we found that MALAT1 enhanced endothelial cell proliferation and tube formation *in vitro*. The *in vivo* results further confirmed that MALAT1 promoted endothelial proliferation, vasculature reconstruction and cerebral perfusion recovery after CCI.

We predicted a series of MALAT1 downstream effectors using bioinformatics software. Among these candidates, EZH2 was selected for subsequent experiments for two reasons: 1) EZH2 exhibited a high affinity for MALAT1 and 2) EZH2 was previously reported to regulate vascular function (Crea et al., 2012). As expected, RNA-pull down assays indicated the direct binding of MALAT1 and EZH2 *in vitro*, which was consistent with previous results (Tee et al., 2016; Kim et al., 2017; Yu et al., 2017b; Wang et al., 2018; Hu et al., 2019). The signaling activated by MALAT1-EZH2 interactions was closely dependent on EZH2 function. EZH2, a catalytic subunit of polycomb repressive complex 2, silences gene transcription via the trimethylation of histone H3 on lysine 27 (H3K27me3). Previous reports indicated that MALAT1 recruits polycomb repressive complex 2 to the promoter region of target genes to enhance H3K27me3 activity, thereby epigenetically inhibiting gene transcription, mainly in cancer and sepsis (Wang et al., 2015; Huo et al., 2017; Lin et al., 2019; Yong et al., 2020). However, in human immunodeficiency virus type 1 (HIV-1)-infected CD4⁺ T cells, MALAT1 inhibited EZH2 from binding to the HIV-1 long terminal repeat promoter, thereby preventing polycomb repressive complex 2-mediated H3K27me3 and alleviating the epigenetic silencing of HIV-1 transcription (Qu et al., 2019). More intriguingly, recent evidence showed that EZH2 also potentiates transcriptional activation (Lee et al., 2011; Xu et al., 2012; Asangani et al., 2013), likely independent of its catalytic H3K27me3 activity. One study found that the amino-terminal HII domain of EZH2 mediated binding to the NOTCH1 promoter and induced its epigenetic activation in breast stem cells (Gonzalez et al., 2014). Similarly, NOTCH1 signaling was suppressed by an EZH2 inhibitor in cultured endothelial cells in our study. It is well documented that the NOTCH1 signaling pathway is a key regulator of tumor angiogenesis via crosstalk with the VEGF/VEGFR system (Kangsamaksin et al., 2014). However, whether MALAT1 influences the expression or activity of EZH2 remains unclear. Our study revealed that MALAT1 enhanced the expression of EZH2 and NOTCH1, and EZH2 rescued the effects of MALAT1 on NOTCH1. Thus, NOTCH1 is regulated by MALAT1, likely through EZH2. NOTCH1 activation reversed the MALAT1 deficiency-mediated impairment of angiogenesis. These findings suggest that the biological action of MALAT1 involves NOTCH1 signaling.

Experimental animal articles revealed that new vessel sprouts and increased capillary density are detected at a relatively short time after brain injury (Park et al., 2009; Hayward et al., 2011; Salehi et

al., 2017). Sprouting angiogenesis may promote neurologic recovery after TBI (Li et al., 2012). Clinical studies also reported that there was a tendency to increase both the number of blood vessels and blood vessels area fraction after brain injury, which may benefit the clinical outcome following TBI (Li et al., 2016; Kobek et al., 2018). In our study, we investigated the potential role of MALAT1 in brain tissue, which showed the highest expression among lncRNAs. Regarding endothelial function, our results demonstrate that MALAT1 promoted angiogenesis via the EZH2-NOTCH1 axis, which may benefit neurological function recovery following TBI. However, due to the species differences between mice and humans, pre-clinical trials are required to perform before it is applied to the clinic.

Acknowledgments: We express special gratitude to the Chongqing Key Laboratory of Neurology for providing the experimental platform. We thank Professor Yan Wang (Chongqing Medical University, China) for proofreading this paper.

Author contributions: Study conception and design, and manuscript drafting: NW, CJC, HL; data collection: JJZ, JCH, ZSZ; data analysis and interpretation: ZGW; manuscript revision: NW, CJC, HL, XCS. All authors read and approved the final manuscript.

Conflicts of interest: The authors declare that there are no conflicts of interest associated with this manuscript.

Open access statement: This is an open access journal, and articles are distributed under the terms of the Creative Commons Attribution NonCommercial-ShareAlike 4.0 License, which allows others to remix, tweak, and build upon the work non-commercially, as long as appropriate credit is given and the new creations are licensed under the identical terms.

©Article author(s) (unless otherwise stated in the text of the article) 2022. All rights reserved. No commercial use is permitted unless otherwise expressly granted.

References

- Akil A, Gutiérrez-García AK, Guenter R, Rose JB, Beck AW, Chen H, Ren B (2021) Notch signaling in vascular endothelial cells, angiogenesis, and tumor progression: an update and prospective. *Front Cell Dev Biol* 9:642352.
- Asangani IA, Ateeq B, Cao Q, Dodson L, Pandhi M, Kunju LP, Mehra R, Lonigro RJ, Siddiqui J, Palanisamy N, Wu YM, Cao X, Kim JH, Zhao M, Qin ZS, Iyer MK, Maher CA, Kumar-Sinha C, Varambally S, Chinnaiyan AM (2013) Characterization of the EZH2-MMSET histone methyltransferase regulatory axis in cancer. *Mol Cell* 49:80-93.
- Beermann J, Piccoli MT, Viereck J, Thum T (2016) Non-coding RNAs in development and disease: background, mechanisms, and therapeutic approaches. *Physiol Rev* 96:1297-1325.
- Brütsch R, Liebler SS, Wüsthube J, Bartol A, Herberich SE, Adam MG, Telzerow A, Augustin HG, Fischer A (2010) Integrin cytoplasmic domain-associated protein-1 attenuates sprouting angiogenesis. *Circ Res* 107:592-601.
- Chen H, Xue LX, Cao HL, Chen SW, Guo Y, Gao WW, Ju SM, Tian HL (2013) Endostatin/collagen XVIII is increased in cerebrospinal fluid after severe traumatic brain injury. *Biomed Res Int* 2013:402375.
- Cheng X, Xu J, Yu Z, Xu J, Long H (2020) LncRNA Xist contributes to endogenous neurological repair after chronic compressive spinal cord injury by promoting angiogenesis through the miR-32-5p/Notch-1 axis. *Front Cell Dev Biol* 8:744.
- Crea F, Fornaro L, Bocci G, Sun L, Farrar WL, Falcone A, Danesi R (2012) EZH2 inhibition: targeting the crossroad of tumor invasion and angiogenesis. *Cancer Metastasis Rev* 31:753-761.
- Daneman R, Prat A (2015) The blood-brain barrier. *Cold Spring Harb Perspect Biol* 7:a020412.
- Delbary-Gossart S, Lee S, Baroni M, Lamarche I, Arnone M, Canolle B, Lin A, Sacramento J, Salegio EA, Castel MN, Delesque-Touchard N, Alam A, Laboudie P, Ferzaz B, Savi P, Herbert JM, Manley GT, Ferguson AR, Bresnahan JC, Bono F, et al. (2016) A novel inhibitor of p75-neurotrophin receptor improves functional outcomes in two models of traumatic brain injury. *Brain* 139:1762-1782.
- Di Y, Wang Y, Wang X, Nie QZ (2021) Effects of long non-coding RNA myocardial infarction-associated transcript on retinal neovascularization in a newborn mouse model of oxygen-induced retinopathy. *Neural Regen Res* 16:1877-1881.
- Diaz-Arrastia R, Kochanek PM, Bergold P, Kenney K, Marx CE, Grimes CJ, Loh LT, Adam LT, Oskvig D, Curley KC, Salzer W (2014) Pharmacotherapy of traumatic brain injury: state of the science and the road forward: report of the Department of Defense Neurotrauma Pharmacology Workgroup. *J Neurotrauma* 31:135-158.
- Fiedler J, Breckwoldt K, Remmele CW, Hartmann D, Dittrich M, Pfanne A, Just A, Xiao K, Kunz M, Müller T, Hansen A, Geffers R, Dandekar T, Eschenhagen T, Thum T (2015) Development of long noncoding RNA-based strategies to modulate tissue vascularization. *J Am Coll Cardiol* 66:2005-2015.
- Flierl MA, Stahel PF, Beauchamp KM, Morgan SJ, Smith WR, Shohami E (2009) Mouse closed head injury model induced by a weight-drop device. *Nat Protoc* 4:1328-1337.
- Gonzalez ME, Moore HM, Li X, Toy KA, Huang W, Sabel MS, Kidwell KM, Kleer CG (2014) EZH2 expands breast stem cells through activation of NOTCH1 signaling. *Proc Natl Acad Sci U S A* 111:3098-3103.
- Hayward NM, Tuunanen PI, Immonen R, Ndode-Ekane XE, Pitkänen A, Gröhn O (2011) Magnetic resonance imaging of regional hemodynamic and cerebrovascular recovery after lateral fluid-percussion brain injury in rats. *J Cereb Blood Flow Metab* 31:166-177.
- Hu H, Wu J, Yu X, Zhou J, Yu H, Ma L (2019) Long non-coding RNA MALAT1 enhances the apoptosis of cardiomyocytes through autophagy inhibition by regulating TSC2-mTOR signaling. *Biol Res* 52:58.
- Huang M, Hou J, Wang Y, Xie M, Wei C, Nie F, Wang Z, Sun M (2017) Long noncoding RNA LINC00673 is activated by SP1 and exerts oncogenic properties by interacting with LSD1 and EZH2 in gastric cancer. *Mol Ther* 25:1014-1026.
- Huang Z, Cheng C, Jiang L, Yu Z, Cao F, Zhong J, Guo Z, Sun X (2016) Intraventricular apolipoprotein ApoJ infusion acts protectively in traumatic brain injury. *J Neurochem* 136:1017-1025.
- Huo Y, Li Q, Wang X, Jiao X, Zheng J, Li Z, Pan X (2017) MALAT1 predicts poor survival in osteosarcoma patients and promotes cell metastasis through associating with EZH2. *Oncotarget* 8:46993-47006.
- Jaé N, Dimmeler S (2015) Long noncoding RNAs in diabetic retinopathy. *Circ Res* 116:1104-1106.
- Ji P, Diederichs S, Wang W, Böing S, Metzger R, Schneider PM, Tidow N, Brandt B, Burger H, Bulk E, Thomas M, Berdel WE, Serve H, Müller-Tidow C (2003) MALAT-1, a novel noncoding RNA, and thymosin beta4 predict metastasis and survival in early-stage non-small cell lung cancer. *Oncogene* 22:8031-8041.
- Jiang Y, Brody DL (2012) Administration of COG1410 reduces axonal amyloid precursor protein immunoreactivity and microglial activation after controlled cortical impact in mice. *J Neurotrauma* 29:2332-2341.
- Joris PJ, Mensink RP, Adam TC, Liu TT (2018) Cerebral blood flow measurements in adults: a review on the effects of dietary factors and exercise. *Nutrients* 10:530.
- Kangsamaksn T, Tattersall IW, Kitajewski J (2014) Notch functions in developmental and tumour angiogenesis by diverse mechanisms. *Biochem Soc Trans* 42:1563-1568.
- Kim SH, Kim SH, Yang WI, Kim SJ, Yoon SO (2017) Association of the long non-coding RNA MALAT1 with the polycomb repressive complex pathway in T and NK cell lymphoma. *Oncotarget* 8:31305-31317.
- Kobek M, Jankowski Z, Szala J, Gąsczyk-Ożarowski Z, Pałasz A, Skowronek R (2018) Time-related morphometric studies on CD34 protein expression in the cerebral blood vessels after fatal brain contusions. *Folia Neuropathol* 56:187-195.
- Lee JB, Werbowetski-Ogilvie TE, Lee JH, McIntyre BA, Schnerch A, Hong SH, Park IH, Daley GQ, Bernstein ID, Bhatia M (2013) Notch-HES1 signaling axis controls hematopoietic fate decisions of human embryonic and induced pluripotent stem cells. *Blood* 122:1162-1173.
- Lee ST, Li Z, Wu Z, Aau M, Guan P, Karuturi RK, Liou YC, Yu Q (2011) Context-specific regulation of NF-κB target gene expression by EZH2 in breast cancers. *Mol Cell* 43:798-810.
- Leisegang MS, Fork C, Josipovic I, Richter FM, Preussner J, Hu J, Miller MJ, Epah J, Hofmann P, Günther S, Moll F, Valasarajan C, Heidler J, Ponomareva Y, Freiman TM, Maedgessell L, Plate KH, Mittelbronn M, Uchida S, Künne C, et al. (2017) Long noncoding RNA MANTIS facilitates endothelial angiogenic function. *Circulation* 136:65-79.
- Li L, Chopp M, Ding GL, Qu CS, Li QJ, Lu M, Wang S, Nejad-Davarani SP, Mahmood A, Jiang Q (2012) MRI measurement of angiogenesis and the therapeutic effect of acute marrow stromal cell administration on traumatic brain injury. *J Cereb Blood Flow Metab* 32:2023-2032.
- Li M, Jia Q, Chen T, Zhao Z, Chen J, Zhang J (2016) The role of vascular endothelial growth factor and vascular endothelial growth inhibitor in clinical outcome of traumatic brain injury. *Clin Neurol Neurosurg* 144:7-13.
- Li P, Gan Y, Sun BL, Zhang F, Lu B, Gao Y, Liang W, Thomson AW, Chen J, Hu X (2013) Adoptive regulatory T-cell therapy protects against cerebral ischemia. *Ann Neurol* 74:458-471.
- Liang YH, Chen GW, Li XS, Jia S, Meng CY (2021) Guanosine-5'-triphosphate cyclohydrolase 1 regulated long noncoding RNAs are potential targets for microglial activation in neuropathic pain. *Neural Regen Res* 16:596-600.
- Lin N, Yao Z, Xu M, Chen J, Lu Y, Yuan L, Zhou S, Zou X, Xu R (2019) Long noncoding RNA MALAT1 potentiates growth and inhibits senescence by antagonizing ABI3BP in gallbladder cancer cells. *J Exp Clin Cancer Res* 38:244.
- Liu H, He J, Zhang Z, Liu L, Huo G, Sun X, Cheng C (2018) Evolution of cerebral perfusion in the peri-contusional cortex in mice revealed by in vivo laser speckle imaging after traumatic brain injury. *Brain Res* 1700:118-125.

- Mao L, Li P, Zhu W, Cai W, Liu Z, Wang Y, Luo W, Stetler RA, Leak RK, Yu W, Gao Y, Chen J, Chen G, Hu X (2017) Regulatory T cells ameliorate tissue plasminogen activator-induced brain haemorrhage after stroke. *Brain* 140:1914-1931.
- Michalik KM, You X, Manavski Y, Doddaballapur A, Zörnig M, Braun T, John D, Ponomareva Y, Chen W, Uchida S, Boon RA, Dimmeler S (2014) Long noncoding RNA MALAT1 regulates endothelial cell function and vessel growth. *Circ Res* 114:1389-1397.
- Mueller CA, Schluesener HJ, Fauser U, Conrad S, Schwab JM (2007) Lesional expression of the endogenous angiogenesis inhibitor endostatin/collagen XVIII following traumatic brain injury (TBI). *Exp Neurol* 208:228-237.
- Park E, Bell JD, Siddiq IP, Baker AJ (2009) An analysis of regional microvascular loss and recovery following two grades of fluid percussion trauma: a role for hypoxia-inducible factors in traumatic brain injury. *J Cereb Blood Flow Metab* 29:575-584.
- Percie du Sert N, Hurst V, Ahluwalia A, Alam S, Avey MT, Baker M, Browne WJ, Clark A, Cuthill IC, Dirnagl U, Emerson M, Garner P, Holgate ST, Howells DW, Karp NA, Lazic SE, Lidster K, MacCallum CJ, Macleod M, Pearl EJ, et al. (2020) The ARRIVE guidelines 2.0: updated guidelines for reporting animal research. *J Physiol* 598:3793-3801.
- Qu D, Sun WW, Li L, Ma L, Sun L, Jin X, Li T, Hou W, Wang JH (2019) Long noncoding RNA MALAT1 releases epigenetic silencing of HIV-1 replication by displacing the polycomb repressive complex 2 from binding to the LTR promoter. *Nucleic Acids Res* 47:3013-3027.
- Ren B, Rose JB, Liu Y, Jaskular-Sztul R, Contreras C, Beck A, Chen H (2019) Heterogeneity of vascular endothelial cells, de novo arteriogenesis and therapeutic implications in pancreatic neuroendocrine tumors. *J Clin Med* 8:1980.
- Ren C, Yao Y, Han R, Huang Q, Li H, Wang B, Li S, Li M, Mao Y, Mao X, Xie L, Zhou L, Hu J, Ji X, Jin K (2018) Cerebral ischemia induces angiogenesis in the peri-infarct regions via Notch1 signaling activation. *Exp Neurol* 304:30-40.
- Salehi A, Zhang JH, Obenaus A (2017) Response of the cerebral vasculature following traumatic brain injury. *J Cereb Blood Flow Metab* 37:2320-2339.
- Schmid MC, Avraamides CJ, Foubert P, Shaked Y, Kang SW, Kerbel RS, Varner JA (2011) Combined blockade of integrin- $\alpha 4\beta 1$ plus cytokines SDF-1 α or IL-1 β potentially inhibits tumor inflammation and growth. *Cancer Res* 71:6965-6975.
- Sköld MK, Risling M, Holmin S (2006) Inhibition of vascular endothelial growth factor receptor 2 activity in experimental brain contusions aggravates injury outcome and leads to early increased neuronal and glial degeneration. *Eur J Neurosci* 23:21-34.
- Sköld MK, von Gertten C, Sandberg-Nordqvist AC, Mathiesen T, Holmin S (2005) VEGF and VEGF receptor expression after experimental brain contusion in rat. *J Neurotrauma* 22:353-367.
- Stein SC, Georgoff P, Meghan S, Mizra K, Sonnad SS (2010) 150 years of treating severe traumatic brain injury: a systematic review of progress in mortality. *J Neurotrauma* 27:1343-1353.
- Sun M, Kraus WL (2015) From discovery to function: the expanding roles of long noncoding RNAs in physiology and disease. *Endocr Rev* 36:25-64.
- Tee AE, Liu B, Song R, Li J, Pasquier E, Cheung BB, Jiang C, Marshall GM, Haber M, Norris MD, Fletcher JJ, Dinger ME, Liu T (2016) The long noncoding RNA MALAT1 promotes tumor-driven angiogenesis by up-regulating pro-angiogenic gene expression. *Oncotarget* 7:8663-8675.
- Thum T, Fiedler J (2014) LINCing MALAT1 and angiogenesis. *Circ Res* 114:1366-1368.
- Tuschcherer G, Servis C, Corradin G, Blum U, Rivier J, Mutter M (1992) Total chemical synthesis, characterization, and immunological properties of an MHC class I model using the TASP concept for protein de novo design. *Protein Sci* 1:1377-1386.
- van Kruijsdijk RC, van der Graaf Y, Algra A, de Borst GJ, Cramer MJ, Siersema PD, Peeters PH, Visseren FL, SMART study group (2016) The effects of secondary cardiovascular prevention on cancer risk in patients with manifest vascular disease. *J Am Coll Cardiol* 68:2588-2589.
- Wan W, Hou Y, Wang K, Cheng Y, Pu X, Ye X (2019) The LXR-623-induced long non-coding RNA LINC01125 suppresses the proliferation of breast cancer cells via PTEN/AKT/p53 signaling pathway. *Cell Death Dis* 10:248.
- Wang C, Qu Y, Suo R, Zhu Y (2019) Long non-coding RNA MALAT1 regulates angiogenesis following oxygen-glucose deprivation/reoxygenation. *J Cell Mol Med* 23:2970-2983.
- Wang CF, Zhao CC, Weng WJ, Lei J, Lin Y, Mao Q, Gao GY, Feng JF, Jiang JY (2017) Alteration in long non-coding RNA expression after traumatic brain injury in rats. *J Neurotrauma* 34:2100-2108.
- Wang D, Ding L, Wang L, Zhao Y, Sun Z, Karnes RJ, Zhang J, Huang H (2015) LncRNA MALAT1 enhances oncogenic activities of EZH2 in castration-resistant prostate cancer. *Oncotarget* 6:41045-41055.
- Wang G, Jiang X, Pu H, Zhang W, An C, Hu X, Liou AK, Leak RK, Gao Y, Chen J (2013) Scriptaid, a novel histone deacetylase inhibitor, protects against traumatic brain injury via modulation of PTEN and AKT pathway: scriptaid protects against TBI via AKT. *Neurotherapeutics* 10:124-142.
- Wang Y, Xie Y, Li L, He Y, Zheng D, Yu P, Yu L, Tang L, Wang Y, Wang Z (2018) EZH2 RIP-seq identifies tissue-specific long non-coding RNAs. *Curr Gene Ther* 18:275-285.
- Williams CK, Li JL, Murga M, Harris AL, Tosato G (2006) Up-regulation of the Notch ligand Delta-like 4 inhibits VEGF-induced endothelial cell function. *Blood* 107:931-939.
- Wright DW, Yeatts SD, Silbergleit R, Palesch YY, Hertzberg VS, Frankel M, Goldstein FC, Caveney AF, Howlett-Smith H, Bengelink EM, Manley GT, Merck LH, Janis LS, Barsan WG; NETT Investigators (2014) Very early administration of progesterone for acute traumatic brain injury. *N Engl J Med* 371:2457-2466.
- Xu K, Wu ZJ, Groner AC, He HH, Cai C, Lis RT, Wu X, Stack EC, Loda M, Liu T, Xu H, Cato L, Thornton JE, Gregory RI, Morrissey C, Vessella RL, Montironi R, Magi-Galluzzi C, Kantoff PW, Balk SP, et al. (2012) EZH2 oncogenic activity in castration-resistant prostate cancer cells is Polycomb-independent. *Science* 338:1465-1469.
- Yang LX, Yang LK, Zhu J, Chen JH, Wang YH, Xiong K (2019) Expression signatures of long non-coding RNA and mRNA in human traumatic brain injury. *Neural Regen Res* 14:632-641.
- Yao RW, Wang Y, Chen LL (2019) Cellular functions of long noncoding RNAs. *Nat Cell Biol* 21:542-551.
- Yin KJ, Fan Y, Hamblin M, Zhang J, Zhu T, Li S, Hawse JR, Subramaniam M, Song CZ, Urrutia R, Lin JD, Chen YE (2013) KLF11 mediates PPAR γ cerebrovascular protection in ischaemic stroke. *Brain* 136:1274-1287.
- Yin KJ, Cirrito JR, Yan P, Hu X, Xiao Q, Pan X, Bateman R, Song H, Hsu FF, Turk J, Xu J, Hsu CY, Mills JC, Holtzman DM, Lee JM (2006) Matrix metalloproteinases expressed by astrocytes mediate extracellular amyloid-beta peptide catabolism. *J Neurosci* 26:10939-10948.
- Yong H, Wu G, Chen J, Liu X, Bai Y, Tang N, Liu L, Wei J (2020) lncRNA MALAT1 accelerates skeletal muscle cell apoptosis and inflammatory response in sepsis by decreasing BRCA1 expression by recruiting EZH2. *Mol Ther Nucleic Acids* 21:1120-1121.
- Yu Y, Cao F, Ran Q, Wang F (2017a) Long non-coding RNA Gm4419 promotes trauma-induced astrocyte apoptosis by targeting tumor necrosis factor α . *Biochem Biophys Res Commun* 491:478-485.
- Yu Z, Rayile A, Zhang X, Li Y, Zhao Q (2017b) Ulinastatin protects against lipopolysaccharide-induced cardiac microvascular endothelial cell dysfunction via downregulation of lncRNA MALAT1 and EZH2 in sepsis. *Int J Mol Med* 39:1269-1276.
- Zhang X, Tang X, Hamblin MH, Yin KJ (2018) Long non-coding RNA Malat1 regulates angiogenesis in hindlimb ischemia. *Int J Mol Sci* 19:1723.
- Zhang X, Tang X, Liu K, Hamblin MH, Yin KJ (2017) Long noncoding RNA Malat1 regulates cerebrovascular pathologies in ischemic stroke. *J Neurosci* 37:1797-1806.
- Zhang Y, Wang J, Zhang Y, Wei J, Wu R, Cai H (2019) Overexpression of long noncoding RNA Malat1 ameliorates traumatic brain injury induced brain edema by inhibiting AQP4 and the NF- κ B/IL-6 pathway. *J Cell Biochem* 120:17584-17592.
- Zhong J, Jiang L, Cheng C, Huang Z, Zhang H, Liu H, He J, Cao F, Peng J, Jiang Y, Sun X (2016) Altered expression of long non-coding RNA and mRNA in mouse cortex after traumatic brain injury. *Brain Res* 1646:589-600.
- Zhong J, Jiang L, Huang Z, Zhang H, Cheng C, Liu H, He J, Wu J, Darwazeh R, Wu Y, Sun X (2017) The long non-coding RNA Neat1 is an important mediator of the therapeutic effect of bexarotene on traumatic brain injury in mice. *Brain Behav Immun* 65:183-194.
- Zhou C, Chen H, Zheng JF, Guo ZD, Huang ZI, Wu Y, Zhong JJ, Sun XC, Cheng CJ (2020) Pentraxin 3 contributes to neurogenesis after traumatic brain injury in mice. *Neural Regen Res* 15:2318-2326.
- Zhu Y, Lee C, Shen F, Du R, Young WL, Yang GY (2005) Angiotensin-2 facilitates vascular endothelial growth factor-induced angiogenesis in the mature mouse brain. *Stroke* 36:1533-1537.

C-Editor: Zhao M; S-Editors: Yu J, Li CH; L-Editors: Crawford M, Yu J, Song LP; T-Editor: Jia Y